ELSEVIER

Journal of Alloys and Compounds 317–318 (2001) 250–253

Journal of ALLOYS AND COMPOUNDS

www.elsevier.com/locate/jallcom

Structural chemistry, magnetic and electrical properties of ternary rare-earth nickel phosphides, $R_{20}Ni_{42}P_{30}$ (R=Ce, Sm)

V. Babizhetskyy, F. Weitzer, K. Hiebl*

Institut fürPhysikalische Chemie der Universität Wien, Währingerstraße 42, A-1090 Wien, Austria

Abstract

We have investigated the magnetic and electrical transport properties of two ternary compounds $R_{20}Ni_{42}P_{30}$ (R=Ce, Sm), which crystallize in the hexagonal $Sm_{20}Ni_{41.6}P_{30}$ structure type, space group $P6_3/m$. Both samples undergo magnetic transitions below 50 K. The cerium atom adopts an intermediate valence state ($v \sim 3.8$). The temperature dependence of the resistivity, ρ, of $Sm_{20}Ni_{42}P_{30}$ resembles the shape of a simple non-magnetic metal, whereas $\rho(T)$ of $Ce_{20}Ni_{42}P_{30}$ reveals the typical feature of a Kondo lattice.

Keywords: Ternary rare-earth nickel phosphides; Crystal structure; Magnetism; Electrical resistivity

1. Introduction

Many ternary compounds composed of a rare-earth element (R=Sc, Y, La–Lu), transition metal (T=3d, 4d and 5d elements) and phosphorous have been synthesized and structurally identified over the past decades. The magnetic behavior has been less intensively studied and the electric transport properties have hardly been measured at all so far [1]. Hence the investigation of the physical properties of the compounds $Ce_{20}Ni_{42}P_{30}$ and $Sm_{20}Ni_{42}P_{30}$ [2,3] became the subject of this work.

2. Experimental details

Polycrystalline samples of the ternary compounds $R_{20}Ni_{42}P_{30}$ (R=Ce, Sm) were prepared from pure elements: Both red phosphorus and nickel 99.99% were supplied by Johnson Matthey, Karlsruhe, Germany and the rare-earth metals ingots 99.9% were obtained from Strem Chemicals, Karlsruhe, Germany. Stoichiometric amounts of powder and filed chips of the constituents were mixed together and pressed into pellets. A small excess of phosphorus (~0.1 g) was added to compensate for evaporation losses during the arc melting process. Prior to the melting in an arc furnace under high purity argon the pellets were pre-reacted in evacuated silica tubes by gradually heating up to 1070 K, keeping them at this temperature for 1 day and slowly cooling down. Then, in order to reach thermodynamic equilibrium, the so-obtained samples were again sealed in evacuated silica tubes, heat treated for 1 month at 1070 K and subsequently quenched by submerging in cold water.

Precise lattice parameters were derived by the least squares refinement of room temperature Image Plate Huber, Rimsling, Germany, G 670 X-ray powder diffractometer data ($8° \leq 2\theta \leq 100°$, stepsize=0.005°) with monochromatic Cu $K\alpha_1$ radiation. Germanium (99.9999%, $a_{Ge}=0.5657905$ nm) served as the internal standard.

The magnetic properties were studied by use of a Faraday balance, SUS-10, A. Paar, Graz, Austria, in the temperature range 80–500 K and in external fields up to 1.3 T, a Lake-Shore, Westerville, Ohio, USA, AC susceptometer, AC 7000 ($f=133.3$ Hz, $B_{AC}=1$ mT) for temperatures 4.2 K$<T<$100 K.

Measurements of the electrical resistivity were performed applying a common four probe Lake-Shore AC resistivity option ($f=133.3$ Hz, $i_{AC}=10$ mA) in the temperature range 4.2–300 K. The annealed buttons were cut by a diamond saw (Bühler Isomet, Leoben, Austria) into bar-shaped samples with the approximate dimensions of $1\times1\times5$ mm^3. Electrical contacts were made using

*Corresponding author. Tel.: +43-1-4277-52422; fax: +43-1-4277-9524.
E-mail address: kurt.hiebl@univie.ac.at (K. Hiebl).

0925-8388/01/$ – see front matter
PII: S0925-8388(00)01342-6

commercial silver paint (Degussa, Hanau, Germany) and 25-μ gold wire.

3. Results and discussion

3.1. Structural characterization

The X-ray powder patterns of the ternary compounds $R_{20}Ni_{42}P_{30}$ were indexed on the basis of the $Sm_{20}Ni_{41.6}P_{30}$-structure type [2] hexagonal unit cell, space group $P6_3/m$. The following lattice parameters for $Sm_{20}Ni_{42}P_{30}$ have been calculated; $a = 20.4271(2)$ Å and $c = 3.86514(4)$ Å. A Rietveld-type profile refinement was performed for the compound $Ce_{20}Ni_{42}P_{30}$, using the program Fullprof [4] to check the crystallographic structure and the atomic positions. Fig. 1 shows the final fit obtained between calculated and observed patterns. Details of the refinement are summarized in Table 1 and final atom parameters are given in Table 2.

Table 1
Rietveld-refinement data of $Ce_{20}Ni_{42}P_{30}$

Formula	$Ce_{20}Ni_{42}P_{30}$
Space group	$P6_3/m$, No 176
Radiation wavelength Cu $K\alpha_1$(Å)	1.54056
Lattice parameters (Å)	
a	20.4620(4)
c	3.89184(8)
Unit-cell volume (Å^3)	1410.93(8)
Calculated density (kg/m^3)	7.3660(4)
Formula per unit cell	$Z = 1$
Scan range	$25° < 2\theta < 100°$
Step size (2θ)	0.005
Node of refinement	Full profile
Number of fitted parameters	59
Residual values	
R_p	0.17
R_{wp}	0.15
R_B	0.098
R_F	0.079

3.2. Magnetism

The reciprocal susceptibilities versus temperature for both compounds $Ce_{20}Ni_{42}P_{30}$ and $Sm_{20}Ni_{42}P_{30}$ are shown in Figs. 2 and 3. Above approximately 50 K, the measured data do not follow a linear Curie–Weiss law and the values for the effective moments, μ_{eff}, as well as the paramagnetic Curie temperatures, Θ_p, were calculated using the modified formula:

$$\chi = \frac{C}{T - \Theta_p} + \chi_o \quad (1)$$

C being the Curie constant and χ_o denoting temperature independent contributions such as core diamagnetism, Landau diamagnetism and Pauli paramagnetism. The derived values in case of the cerium containing compound are: $\mu_{eff} = 1\ \mu_B$, $\Theta_p = 29$ K and $\chi_o = 1.03$ cm^3/mol. The reduced moment is an indication that the cerium ion possibly adopts an intermediate valence state due to Kondo-like (see below) valence fluctuations. Hence a predominantly tetravalent behavior for cerium is suggested with only a small fraction (15–20%) of Ce^{3+}. Upon lowering the temperature a maximum in the real part of the dynamic susceptibility curve (see inset Fig. 2) is encountered at $T = 32$ K stemming from a magnetic ordering of the Ce^{3+} sublattice. The nature of the magnetic order is yet not clearly understood, since the practically temperature independent imaginary part of the susceptibility favors an antiferromagnetic coupling of the minority spins. The positive Θ_p, however, suggests ferromagnetism. The magnetic data for $Sm_{20}Ni_{42}P_{30}$ are the following: $\mu_{eff} = 0.5\ \mu_B$

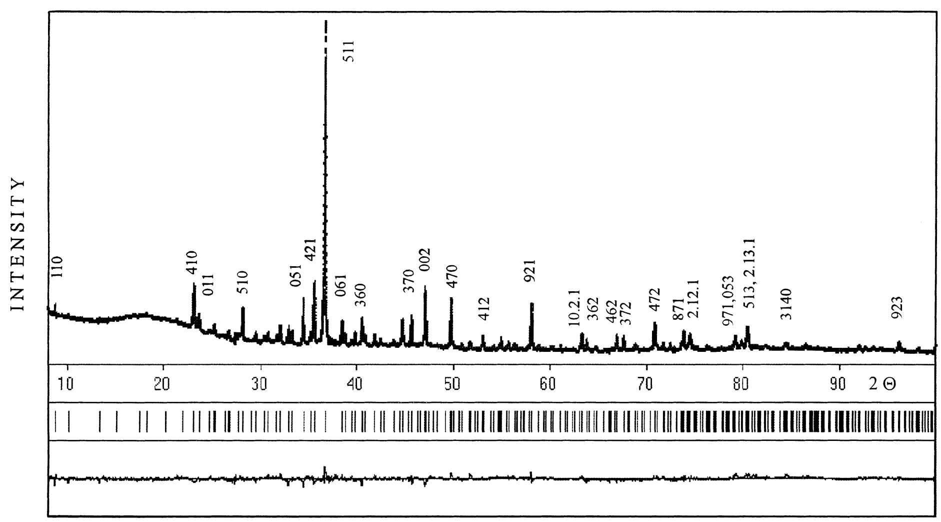

Fig. 1. Observed and calculated profiles of $Ce_{20}Ni_{42}P_{30}$ and the differences between them.

Table 2
Positional and thermal parameters for $Ce_{20}Ni_{42}P_{30}$

Atom	Position	x/a	y/b	z/c	B_{iso}(Å^2)
Ce1	2c	1/3	2/3	1/4	0.4(2)
Ce2	6h	0.2978(4)	0.8409(4)	1/4	0.5(2)
Ce3	6h	0.5068(5)	0.8764(5)	1/4	0.57(22)
Ce4	6h	0.7161(5)	0.9149(5)	1/4	0.64(22)
Ni1	6h	0.243(1)	0.962(1)	1/4	0.6(3)
Ni2	6h	0.454(1)	0.994(1)	1/4	0.8(5)
Ni3	6h	0.763(1)	0.592(1)	1/4	0.8(4)
Ni4	6h	0.779(1)	0.410(1)	1/4	1.1(6)
Ni5	6h	0.938(1)	0.789(1)	1/4	1.0(4)
Ni6	6h	0.976 (1)	0.634(1)	1/4	0.8(3)
Ni7[a]	6h	0.873(9)	0.963(7)	1/4	1.2(5)
Ni8[a]	6h	0.933(6)	0.980(1)	1/4	1.5(6)
P1	6h	0.668(2)	0.634(1)	1/4	0.57(9)
P2	6h	0.704(1)	0.460(2)	1/4	0.57(9)
P3	6h	0.851(1)	0.835(1)	1/4	0.57(9)
P4	6h	0.888(2)	0.666(1)	1/4	0.57(9)
P5	6h	0.921(1)	0.495(2)	1/4	0.57(9)

[a] Occupancies Ni7=78(4)%; Ni8=22(5)%.

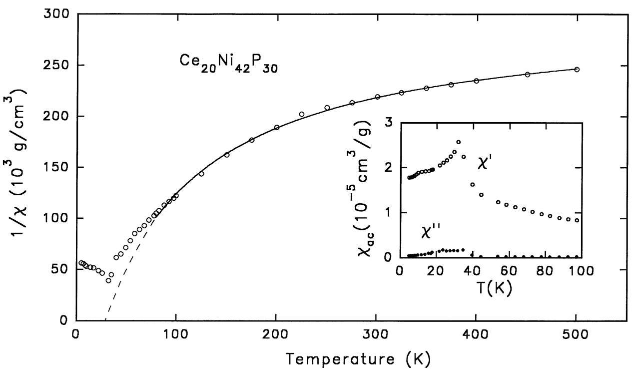

Fig. 2. Reciprocal susceptibility versus temperature for $Ce_{20}Ni_{42}P_{30}$. Solid line calculated according Eq. (1). Inset: dynamic susceptibilities versus temperature.

(which is somewhat smaller than the theoretical value (0.8 μ_B) for Sm^{3+}), $\Theta_p = 35$ K and $\chi_o = 1.16$ cm^3/mol. As can be seen from the inset of Fig. 3 the $\chi'(T)$ plot passes a maximum at the Neél temperature $T_N = 35$ K, χ'' thereby is temperature independent and finally at 10 K a spin reorientation towards a parallel spin alignment is revealed associated with a pronounced increase of both the $\chi'(T)$ and $\chi''(T)$ curves.

3.3. Electrical resistivity

The temperature dependent electrical resistivity of $Sm_{20}Ni_{42}P_{30}$ is shown in Fig. 4 and the $\rho(T)$ curve resembles the typical shape of a metal-like intermetallic compound. As can be seen in the inset of Fig. 4, even in an enlarged scale, the changes of slope at T_{ord} are barely visible, although a first derivative plot $d\rho/dT$ vs. T reveals shallow maxima at $T_N \cong 34$ K and $T_C \cong 6$ K, which are in good accord with magnetic data above. These findings are obviously due to the very small magnetic moment of the Sm atom and thus the influence of the spin disorder resistivity, ρ_{SPD}, to the total resistivity can be neglected. Assuming the validity of Matthiesen's rule, the resistivity of a non-magnetic compound follows the Bloch-Grüneisen relation [5,6]

$$\rho(T) = \rho_0 + 4R\Theta_D\left(\frac{T}{\Theta_D}\right)^5 \int_0^{\Theta_D/T} \frac{x^5\,dx}{(e^x - 1)(1 - e^{-x})} - KT^3 \quad (2)$$

We have fitted our data according Eq. (2) with the following results: residual resistivity ($\rho_o = 211$ μΩ cm), the second, phonon scattering term $\rho_{ph}(T)$ ($R = 0.26$ μΩ cm/K, Debye-temperature, $\Theta_D = 192$ K) and the third term, which is due to the scattering of the conduction electrons into a narrow d band near the Fermi level ($K = 3.3 \times 10^{-7}$ μΩ cm/K^3).

The distinct shape of the $\rho(T)$ plot for $Ce_{20}Ni_{42}P_{30}$, as shown in Fig. 5, is usually taken as an archetypal sign of Kondo interactions. The resistivity curve passes a broad maximum at 67 K, which is generally associated with the Kondo temperature. In order to study the magnetic contri-

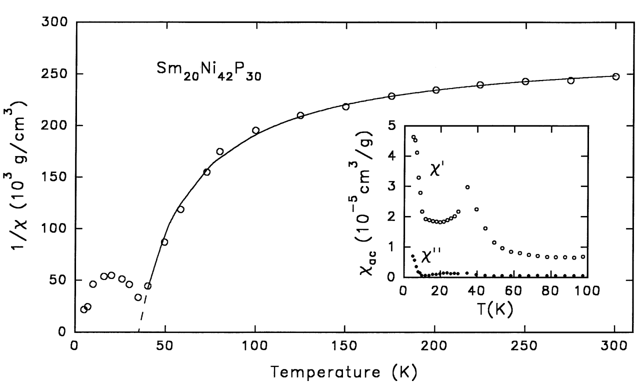

Fig. 3. Reciprocal susceptibility versus temperature for $Sm_{20}Ni_{42}P_{30}$. Solid line calculated according Eq. (1). Inset: dynamic susceptibilities versus temperature.

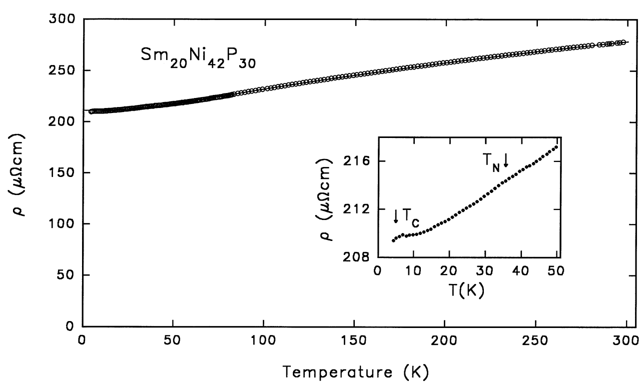

Fig. 4. Electrical resistivity versus temperature for $Sm_{20}Ni_{42}P_{30}$. Solid line calculated according Eq. (2). Inset: low-temperature part of $\rho(T)$, enlarged scale.

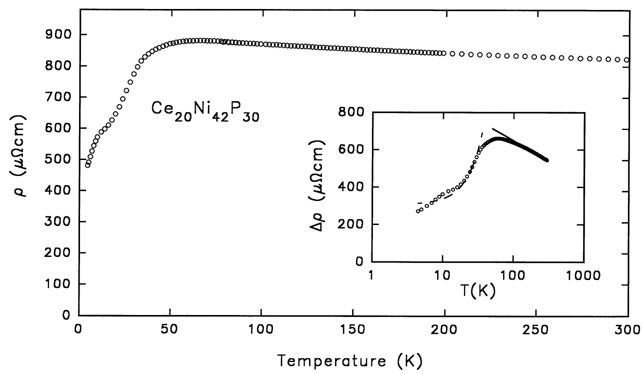

Fig. 5. Electrical resistivity versus temperature for $Ce_{20}Ni_{42}P_{30}$. Inset: semilogarithmic plot of $\rho_{mag}(T)$; dashed line proves T^2 behavior, solid line calculated according Eq. (3).

bution of $\rho(T)$, we have subtracted the data of the 'non-magnetic' $Sm_{20}Ni_{42}P_{30}$ as a reasonable approximation for the phonon contribution to the measured resistivity. The result of $\Delta\rho = \Delta\rho_o + \rho_{mag}$ is presented in a semilogarithmic scale in the inset of Fig. 5. In the lower temperature regime below $T_{ord} = 32$ K a T^2 behavior of the resistivity is observed, the little shoulder is attributed to magnetic impurities, which were not detected in the ac susceptibility. The high temperature ($T > 100$ K) part of ρ_{mag} was analysed in terms of the Kondo theory [7] and we have fitted our data to the standard formula

$$\rho_{mag}(T) = \rho_0^{\infty} - c_K \ln(T) \tag{3}$$

yielding a value of 1080 μΩ cm for the spin disorder resistivity and 94 μΩ cm for the Kondo coefficient, c_K.

Acknowledgements

This research has been sponsored in part by the Austrian Science Foundation (FWF) under grant P 12843-CHE. V.B. is grateful to the FWF providing a Lise Meitner fellowship M546-CHE.

References

[1] Y. Kuz'ma, S. Chykhrij, in: K.A. Gschneidner Jr., L. Eyring (Eds.), Handbook On the Physics and Chemistry of Rare Earths, Vol. 236, Elsevier, Amsterdam, 1996, p. 285.
[2] S. Chykhrij, V. Babizhetskyy, S. Oryshchyn, L. Aksel'rud, Y. Kuz'ma, Kristallografiya 38 (1993) 262.
[3] V. Babizhetskyy, Y. Kuz'ma, Zh. Neorgan. Khimii 39 (1994) 322.
[4] J. Rodriguez-Carvajal, in: Satellite Meeting On Powder Diffraction, 15th Congress of the I.U.C., Toulouse, France, 1990, p. 127, Abstract.
[5] N.F. Mott, H. Jones, The Theory of the Properties of Metals and Alloys, Oxford University Press, London, 1958.
[6] G. Grimvall, The Electron-Phonon Interaction in Metals, North-Holland, Amsterdam, 1981.
[7] J. Kondo, Prog. Theor. Phys. Jpn. 32 (1964) 37.